ChemSusChem

Research Article
doi.org/10.1002/cssc.202300831

Chemistry Europe
European Chemical Societies Publishing

www.chemsuschem.org

DoE-Assisted Development of a 2H–MoS_2-Catalyzed Approach for the Production of Indole Derivatives

Giuseppe Gentile[+],[a] Marc Morant-Giner[+],[a, b] Lucia Cardo,[c] Michele Melchionna,[a] Paolo Fornasiero,[a, d] Maurizio Prato,[a, c, e] and Giacomo Filippini*[a]

2H–MoS_2 is an appealing semiconductor because of its Earth-abundant nature, cheapness, and low toxicity. This material has shown promising catalytic activity for various energy-related processes, but its use in catalysis for C–C bond forming reactions towards useful organic compounds is still largely unexplored. The lack of examples in organic synthesis is mainly due to the intrinsic difficulties of using bulk 2H–MoS_2 (e.g., low surface area), which implies the reliance on high catalytic loadings for obtaining acceptable yields. This makes the optimization process more expensive and tedious. Here, we report the development of a 2H–MoS_2-mediated synthesis of valuable bis(indolyl)methane derivatives, using indoles and benzaldehydes as starting materials. Exploiting the Design of Experiments (DoE) method, we identified the critical parameters affecting the catalytic performance of commercial 2H–MoS_2 powder and optimized the reaction conditions. Lastly, we demonstrated that the catalytic system has versatility and good tolerance towards functional group variations of the reagents.

Introduction

Since the advent of graphene, the scientific community has dedicated tremendous efforts to discover alternative two-dimensional (2D) materials.[1] Among 2D materials, layered transition metal dichalcogenides (TMDCs) represent a family of solid compounds with chemical formula MX_2 (Figure 1a), where M stands for a transition metal (usually belonging to groups IV–VII) and X refers to a chalcogen (such as S, Se, or Te).[2,3] TMDCs show electronic properties that range from semiconducting to superconducting.[4] The bulk structure of layered TMDCs is composed of stacked X–M–X sandwiches, which are held together through van der Waals interactions.[5,6] Because of the weakness of the interlayer interactions in comparison to the intralayer covalent bonding, individual X–M–X slabs (also known as monolayers or single layers) can be isolated in a relatively easy way. The main polytypes are 1T, 2H, and 3R, where the alphanumeric code indicates the number of X–M–X sandwiches per unit cell plus the structural symmetry (H = hexagonal, T = tetragonal, R = rhombohedral).[5] MoS_2 is an archetypical example of layered TMDC with low toxicity.[7] 2H (or 1H in the particular case of the monolayer) and 1T stand out as the most explored types of MoS_2. 2H–MoS_2, with a trigonal prismatic structure, is thermodynamically stable and can be found in nature as molybdenite mineral.[8] When bulk 2H–MoS_2 is downsized to 1H monolayer, it undergoes a transition from

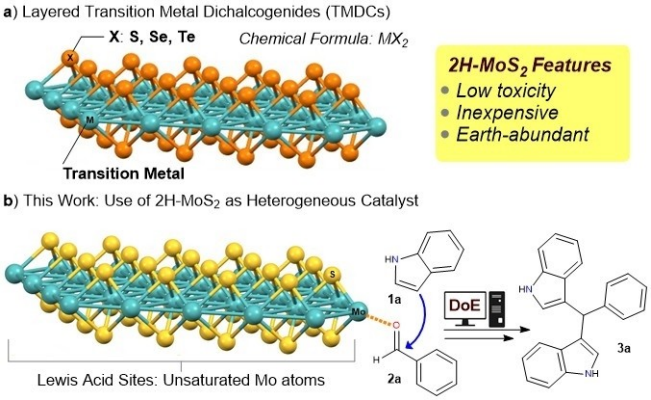

Figure 1. (**a**) General structure of a TMDC layer in its 2H polytype. (**b**) Schematic representation of the reaction between **1a** and **2a** to give **3a** catalysed by 2H–MoS_2 powder. For graphical simplicity, the bulk material used in the manuscript has been represented as a single layer.

[a] G. Gentile,[+] Dr. M. Morant-Giner,[+] Dr. M. Melchionna, Prof. P. Fornasiero, Prof. M. Prato, Dr. G. Filippini
Department of Chemical and Pharmaceutical Sciences, INSTM UdR Trieste
University of Trieste
via Licio Giorgieri 1, 34127, Trieste (Italy)
E-mail: gfilippini@units.it
Homepage: https://pratomaurizio.wixsite.com/labcarbon

[b] Dr. M. Morant-Giner[+]
Instituto de Ciencia Molecular (ICMol)
Universitat de València
C/Catedrático José Beltrán 2, 46980, Paterna (Spain)

[c] Dr. L. Cardo, Prof. M. Prato
Centre for Cooperative Research in Biomaterials (CIC BiomaGUNE)
Basque Research and Technology Alliance (BRTA)
Paseo de Miramón 194, 20014, Donostia-San Sebastián (Spain)

[d] Prof. P. Fornasiero
Istituto di Chimica dei Composti Organometallici – Consiglio Nazionale delle Richerche (ICCOM-CNR)
via Licio Giorgieri 1, 34127, Trieste (Italy)

[e] Prof. M. Prato
Basque Foundation for Science
Ikerbasque, Plaza Euskadi 5, 48013 Bilbao (Spain)

[+] These authors contributed equally to this work.

Supporting information for this article is available on the WWW under https://doi.org/10.1002/cssc.202300831

indirect to direct bandgap.[9] In contrast, 1T–MoS_2, with an octahedral structure, is metastable, not observed in nature, and metallic.[8]

In the vast field of heterogeneous catalysis, (1T-, 2H-, or 1T/2H–)MoS_2, either as pure solid or as part of a nanocomposite, has been proven to be an effective catalytic material in several organic reactions, including nitroarene reduction, crotonaldehyde hydrogenation and disulfide synthesis from carbon disulfide.[10–12] Moreover, MoS_2-based quantum dots have been used to perform the light-driven functionalization of ketones and the cross-dehydrogenative coupling reaction between tertiary amines and suitable nucleophiles.[13,14] In particular, the Lewis acid catalytic sites of 2H–MoS_2 are located at terminal Mo atoms as well as at sulfur vacancies.[15] At these sites, coordinatively unsaturated Mo atoms, with unoccupied d states above the Fermi level, can efficiently interact with electron-donating molecules (*i.e.*, Lewis bases).[16] To amend the typically low surface area of bulk 2H–MoS_2, exfoliation protocols are crucial for boosting the catalytic performance.[10] Additional strategies include vacancy engineering, doping, and preparation of composites or hybrid materials.[10,17]

Besides, MoS_2 and its composite possess all the advantages commonly associated with heterogeneous catalysis including robustness, ease of product separation, and catalyst recycling.[18,19] Despite its interesting catalytic properties, the direct use of 2H–MoS_2 as catalyst in organic synthesis for the formation of new C–C bonds is still rare.[20] Recently, Krishnan and co-workers combined MoS_2 nanosheets with reduced graphene oxide to achieve the functionalization of carbonyl compounds, namely aldehydes and ketones to form bis(indolyl)methane (BIM) derivatives.[20] This class of BIM derivatives are recurrent motifs in numerous terrestrial and marine natural species and exhibit a range of important biological activities.[21–23]

Other commonly applied heterogeneous catalysts for the construction of the BIM scaffold include (*i*) chitosan-supported copper oxide nanoparticles,[24] (*ii*) silica-supported hydrogen sulfate,[25] (*iii*) montmorillonite clay,[26] (*iv*) zeolite,[27] and (*v*) hyper-cross-linked polyaromatic spheres,[22] among others.

However, in the case reported by Krishnan *et al.*, a relatively high loading (up to 50 mg/mL) was necessary for acceptable levels of reactivity. Inspired by this work, we have carried out a thorough investigation to discriminate the critical parameters that define the activity of the commercially available 2H–MoS_2 powder for the reaction between indole **1a** and benzaldehyde **2a** to afford the corresponding bis(indolyl)methane (BIM) derivative **3a** (Figure 1b).

Rather than carrying out a trial-and-error approach, we relied on a rational use of Design of Experiments (DoE) method to optimize the catalysed reaction.[28–30] A commonly overlooked aspect in the optimization of a selected process is the proper understanding of how each variable (from now on, called factor) affects the desired response/s. A conventional method to optimize a process is based on the "One Factor at a Time" (OFAT) approach (Figure 2a). In OFAT optimizations, all factors (X_i) are kept fixed while a selected one (X_1) is variated within the chosen domain to target the desired response/s. Then, that

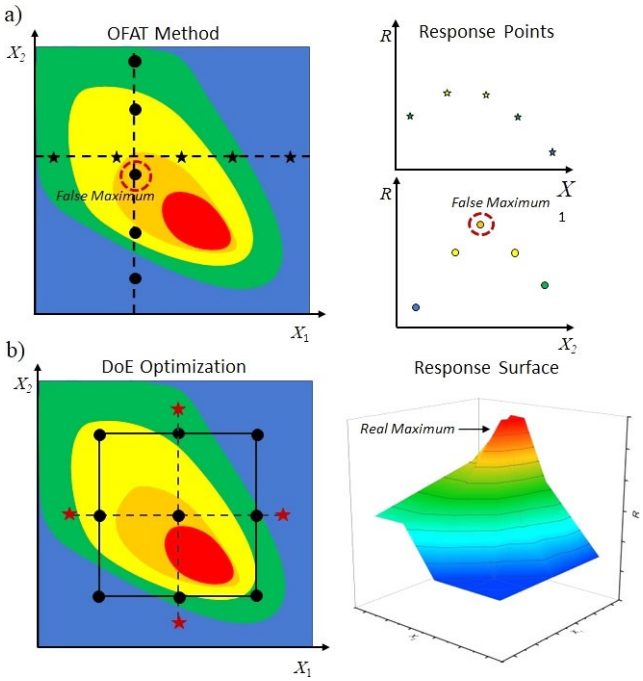

Figure 2. a) Schematic representation of an OFAT approach in a 2D optimization space (*i.e.*, 2 factors). Experiments are aligned along a line representing that just a single factor fluctuates. The response in the reaction space is obtained iteratively by keeping one factor constant while variating the other one. **b**) Schematic representation of a central composite design with star points (DoE optimization). The response is obtained as a response surface along all the reaction space. X: factor; R: response.

factor is fixed again and another one is variated. Thus, through an iterative process, knowledge of the response for a specific process is obtained.[31] Although simple, this methodology is laborious and time-consuming. Indeed, many individual runs, each with just a single modified factor, must be conducted. Accordingly, only point-to-point knowledge can be acquired. Moreover, given the strong dependency on the initial settings of the chosen optimization space, OFAT can mislead users into finding local optima, probably missing the "real" optimal conditions (Figure 2a). Furthermore, pondering the weight of each factor on the response and the possible interactions between factors is difficult, if not impossible. The intrinsic limitations of the OFAT approach could be overcome by the use of "Design of Experiments" (DoE), a statistical approach that generates a model that links mathematically the experimental response to the factors.[32,33] Contrarily to OFAT, DoE permits to vary simultaneously all factors (quantitative or qualitative) in accordance with a predefined experimental matrix (Figure 2b). Subsequently, the data are analysed and a mathematical model is generated, allowing the user to gain a great deal of information on the system under investigation. Thus, DoE is a powerful data analytics tool that permits to screen several variables, their interaction with each other, and the full chemical space. Moreover, it allows to effectively reduce the number of experiments needed to determine which factors have a relevant impact on the selected response.[34–37] For example, Bowden *et al.* reported the use of DoE to accelerate

the optimization of ^{18}F-fluorination of arylstannanes to develop new positron emission tomography (PET) tracers.[37] DoE was proven to be an effective methodology to perform a streamlined optimization process while allowing for multiparametric modelling. Additionally, another example of a successful DoE application has been reported by Carlone and co-workers. The authors, by using a DoE supported rational approach, were able to transfer the enantioselective addition of masked acetaldehyde to nitroalkenes from chloroform to water.[28]

Results and Discussion

DoE optimization studies

In the case of common quantitative factors (temperature, concentration, time, etc.), DoE can be applied in an effective and straightforward way. On the other hand, the optimization of solvent *via* DoE is not a simple task as other statistical tools might be necessary.[38] Consequently, to screen the optimal reaction solvent, an initial OFAT approach was followed (See Figure S3). Specifically, it was found that polar and strong coordinating solvents such as dimethyl sulfoxide (DMSO) and dimethylformamide (DMF) impeded the reaction to take place. When water was used as solvent, compound **3 a** was obtained in low chemical yield (26 ± 3%), since the dispersion of the catalytically active material (2H–MoS_2) in this solvent was modest. Interestingly, less polar solvents, namely ethyl acetate and acetonitrile (MeCN), could homogeneously disperse 2H–MoS_2 while not having a too detrimental coordinating power, thus leading to highest yield of **3 a**. After this solvent screening, acetonitrile, with a yield of 48 ± 4%, was selected as the solvent to perform the next optimization studies.

For this purpose, the software Modde Pro 13.0.2 was used to plan and analyse the experiments. First, the solvent volume was fixed at 1 mL across all runs. Then, five quantitative factors were explored (Figure 3a): (*i*) concentration of **2 a** (0.1, 0.25, 0.5, and 0.75 M); (*ii*) catalyst loading (from 1 to 10 mg/mL); (*iii*) equivalents of **1 a** (from 2 to 4 equivalents); (*iv*) reaction time (2, 4, 6, and 8 h); and (*v*) reaction temperature (25, 35, 50, and 70 °C). A D-optimal design with 26 runs, 3 centre points, and 3 replicated points was selected to construct the experiments matrix. Further details can be consulted in the Supporting Information (S.I.). Importantly, the output summary statistics showed that the model generated fits the experimental data closely. This can be evaluated measuring the fraction of the response variation of the model. This value is indicated by R^2, which is a number comprised between 0 and 1. Specifically, values close to 1 indicate a good level of agreement between the experimental and simulated data. In our case, it was found R^2 equal to 0.98 (see Figure S5). Additionally, the model showed good prediction ability (*i.e.*, the ability to generalize to new and unseen data). The regression coefficients (scaled and centred) can be used to evaluate the significance of each factor on the selected response, specifically the yield of **3 a** (Figure 3b). The model suggested that reaction temperature, concentration of **2 a**, and catalyst loading were significant factors over their investigated ranges (Figure 3b).

The increase of temperature and catalyst loading had a positive effect on the yield of the process, while enhancing the concentration of **2 a** had a negative effect. Conversely, we found that the equivalents of **1 a** and the reaction time were non-significant factors. It was also found that there is a positive interaction between temperature and catalyst loading, while a strong negative quadratic behaviour is detected for the catalyst loading (factor effect plot can be seen in Section 2.3.2 of S.I.). Plotting the response surface across the experimental domain allowed to evaluate and select the optimal reaction conditions (see Figure S9 for complete 4D response contours). In detail, given the negligible effect of the factor "reaction time" over its investigated range, we selected to run the experiment at the 2 h mark. Therefore, this factor was kept constant in the response contours reported in Figure 3c. It was found that a concentration of 0.1 M of **2 a** coupled with a moderate excess of **1 a** (2.75 equiv.) provided the highest yield at the right upper limit of the experimental domain, with a 10 mg/mL of catalyst loading at 70 °C (Figure 3). To validate the model, two points (representing a set of reaction conditions) were extracted from the contour plots at 0.1 M of **2 a** (see Figure S10).[37] In particular, one point was chosen as a "comparison point" to test the efficiency of the different Mo-containing materials (namely, MoS_2, $MoSe_2$, and MoO_2) for the scrutinized reaction. The second point was selected as the "optimized point" to carry out the scope for this reaction. Specifically, the predicted yield for the comparison (50%) was effectively confirmed both by quantitative high-performance liquid chromatography (HPLC) analysis (52 ± 4%) and ^{1}H-NMR determination (51 ± 5%). In the optimized conditions, the predicted yield (90%) was in good agreement with those obtained from HPLC and ^{1}H-NMR measurements (92 ± 2% and 91 ± 3%, respectively). The close match between predicted and observed reaction yields confirmed the robustness of the regression model along with the suitability of the conditions chosen for comparison and to carry out the reaction scope. Once the ideal reaction conditions were rationally defined, we moved to the investigation of the material showing the best activity. As mentioned above, we first evaluated the performance of bulk 2H–MoS_2 that was set as the benchmark catalyst. The nature of 2H polytype was checked by powder X-ray diffraction (PXRD) and Raman spectroscopy (see Section 3.1 of S.I.).

In the wake of the reported ability of TMDCs to interact with molecular species present in the environment,[39,40] we hypothesized that subjecting the 2H–MoS_2 to a "cleaning treatment" would render the Lewis acid sites more accessible to the carbonylic carbon of **2 a**, resulting in boosted catalytic ability. In fact, it is known that the adsorption of molecules alter some of the physical properties of the pristine material.[41,42] Hence, we treated 2H–MoS_2 under vacuum at 50 °C (labelled as MoS_2-50 °C-vac) to remove adsorbates and boost activity. The hypothesis was corroborated by the increment in activity of MoS_2-50 °C-vac as compared to the pristine 2H–MoS_2 (Entries 1–2, Table 1), and with a production rate reaching a value of 5.93 $mmol_{\mathbf{3a}}\, g_{Cat.}^{-1}\, h^{-1}$. This rate also surpasses that of the

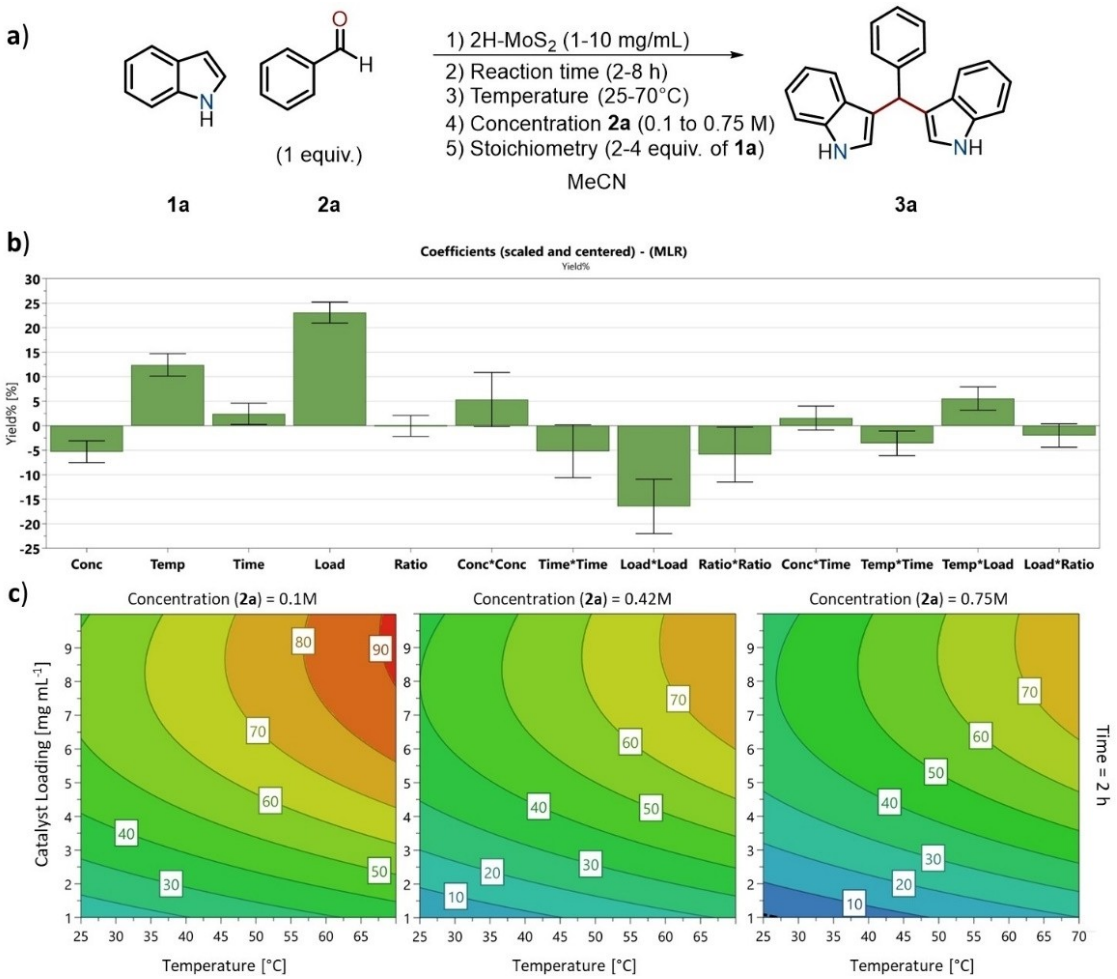

Figure 3. **a**) Investigated factors and their ranges for the D-Optimal optimization study of **3 a** formation. **b**) Scaled and centred regression coefficients calculated from D-Optimal design. Bars with large values have a higher contribution to the response ("Yield%"). A bar with a positive aptitude indicates a factor with a positive influence. On the contrary, a bar with negative aptitude denotes a factor with a diminishing effect on the response. If a factor regression coefficient has an associated error bar greater than its value or it crosses zero, the factor is not significant at the chosen confidence level (specifically 95%). **c**) 4D contour plot outputs: the catalyst loading [mg/mL] is plotted on the vertical axis whereas the temperature [°C] is plotted on the horizontal axis. The three contours, from right to left, show higher concentration of **2 a**. Reaction time is fixed at 2 h and the equivalents of **1 a** are fixed at 2.75. Modde Pro13.0.2 was used to generate the regression coefficient plots and the response contours.

Table 1. Comparison of the catalytic activity of bulk 2H–MoS_2 and treated materials. Reactions were performed on 0.1 mmol scale.

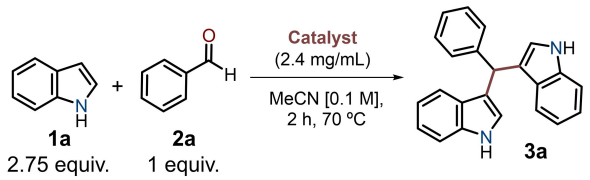

Entry	Catalyst	Yield[a]
1	2H–MoS_2	52 ± 4%
2	MoS_2-50 °C-vac	64 ± 5%
3	$MoSe_2$-50 °C-vac	34 ± 1%
4	MoO_2-50 °C-vac	0%

[a] Yield was calculated via HPLC analysis.

reported benchmark nanocomposite made from MoS_2 nanosheets and reduced graphene oxide, which has a maximum rate of production of 4.40 $mmol_{3a}\, g_{Cat.}^{-1}\, h^{-1}$.[20] The same treatment was also applied to commercially available MoO_2 and $MoSe_2$, thus affording MoO_2-50 °C-vac and $MoSe_2$-50 °C-vac, in order to understand the role of the specific chalcogenide. The lower catalytic activity of $MoSe_2$ (Entry 3, Table 1) can be attributed to the fact that Se atoms are less electronegative and larger than S atoms, resulting in a decreased Lewis acid character of the Mo sites and an increment of the steric hindrance in their vicinity. On the other hand, MoO_2 turned out to be completely inactive for the model reaction (Entry 4, Table 1), presumably as a result of the too hard O^{2-} anion together with the stronger adsorption ability of the MoO_2 in comparison with MoS_2, as also computationally demonstrated, which could saturate the Lewis acid sites.[43]

The catalytic cycle driving the formation of **3 a** is depicted in Scheme 1. The mechanism begins with the activation of **2 a** by

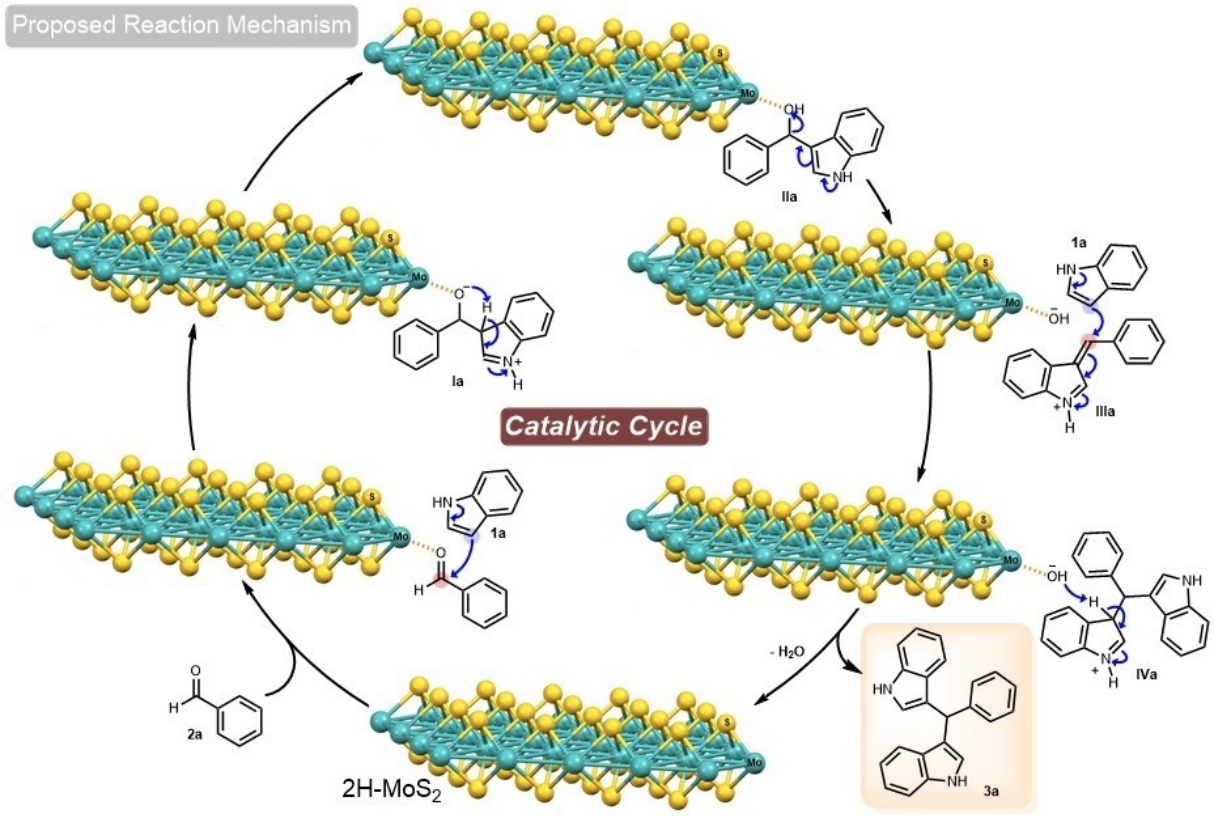

Scheme 1. Proposed reaction mechanism for the reaction between **1 a** and **2 a** to give **3 a**, that is catalysed by 2H–MoS_2 powder. For graphical simplicity, the bulk material used in the manuscript has been represented as a single layer.

the interaction of carbonylic oxygen with the catalytic Lewis acid sites. Then, the condensation between this surface adducts and **1 a** leads to the intermediate **Ia**, which decomposes to the intermediate **IIIa**. Finally, the electrophilic intermediate **IIIa** reacts with a second molecule of **1 a**, eventually affording the **3 a** and the regenerated catalyst.

Characterization of bulk 2H–MoS_2 and MoS_2-50 °C-vac

Bulk 2H–MoS_2 and MoS_2-50 °C-vac were characterized by PXRD, ATR-FTIR (attenuated total reflection Fourier-transform infrared) and Raman spectroscopies, and X-ray photoelectron spectroscopy (XPS). In the PXRD diffractograms of both materials, solely reflections belonging to 2H–MoS_2 are visible, thus ruling out the presence of other crystal phases (Figures S11a and S14a). The ATR-FTIR spectra of both materials only displays a vibrational band at ≈469 cm^{-1}, which is due to Mo–S stretching (Figures S12 and S14b).[44] The Raman spectrum of the commercial powder is dominated by E_{1g}, E^1_{2g}, and A_{1g} modes at ≈285, 380, and 406 cm^{-1}, respectively (Figures 4a and S11b). The value corresponding to the frequency difference between A_{1g} and E^1_{2g} peaks (≈26 cm^{-1}) is consistent with the bulk nature of the material.[45] A similar Raman spectrum is observed in the case of MoS_2-50 °C-vac, confirming that the applied treatment does not cause any phase transition (Figure 4a). Moreover, Brunauer-Emmett-Teller (BET) surface area for bulk 2H–MoS_2 was found to be 10.8 m^2g^{-1}. In relation to the XPS of commercial powder, the Mo 3d spectrum shows Mo^{IV} (from 2H–MoS_2) and Mo^{VI} (from MoO_3) peaks located at ≈229.9/233.0 and 233.0/236.1 eV (Figures 4b and S11c), respectively, while the S 2p spectrum reveals a pair of well-defined peaks (≈162.8 and 163.9 eV) associated to negative divalent sulfide ions (Figures 4c and S11d), in addition to a small S–O contribution (Figure S13).[46] Interestingly, Mo 3d and S 2p spectra of MoS_2-50 °C-vac resemble those of commercial 2H–MoS_2 (Figures 4b and 4c). However, in comparison to the starting 2H–MoS_2, the atomic % of O in MoS_2-50 °C-vac (Table S4), obtained from the XPS survey (Figure S15) is nearly halved. These results prove that the vacuum treatment at 50 °C enables the desorption of oxygen-containing adsorbates (for instance, H_2O molecules) from 2H–MoS_2 surface, without affecting the composition of this TMDC.

Reaction scope

The versatility of MoS_2-50 °C-vac as catalyst for the reaction between **1 a** and different substituted benzaldehydes (**2 a**–**k**) was finally tested (Scheme 2).

In all the entries, the reaction to yield products (**3 a**–**p**) proceeded with good to excellent yields. In particular, the

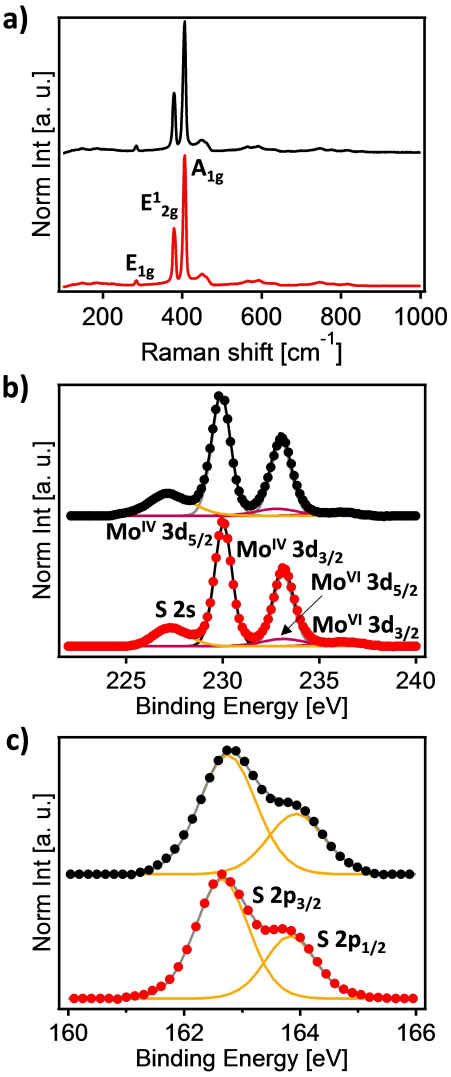

Figure 4. **a**) Normalized Raman spectra of bulk 2H–MoS_2 (in red) and MoS_2-50 °C-vac (in black) normalized respect to the A_{1g} peak of each material (at 532 nm). **b**) Normalized Mo 3d XPS spectra of bulk 2H–MoS_2 (in red) and MoS_2-50 °C-vac (in black). **c**) Normalized S 2p XPS spectra of bulk 2H–MoS_2 (in red) and MoS_2-50 °C-vac (in black).

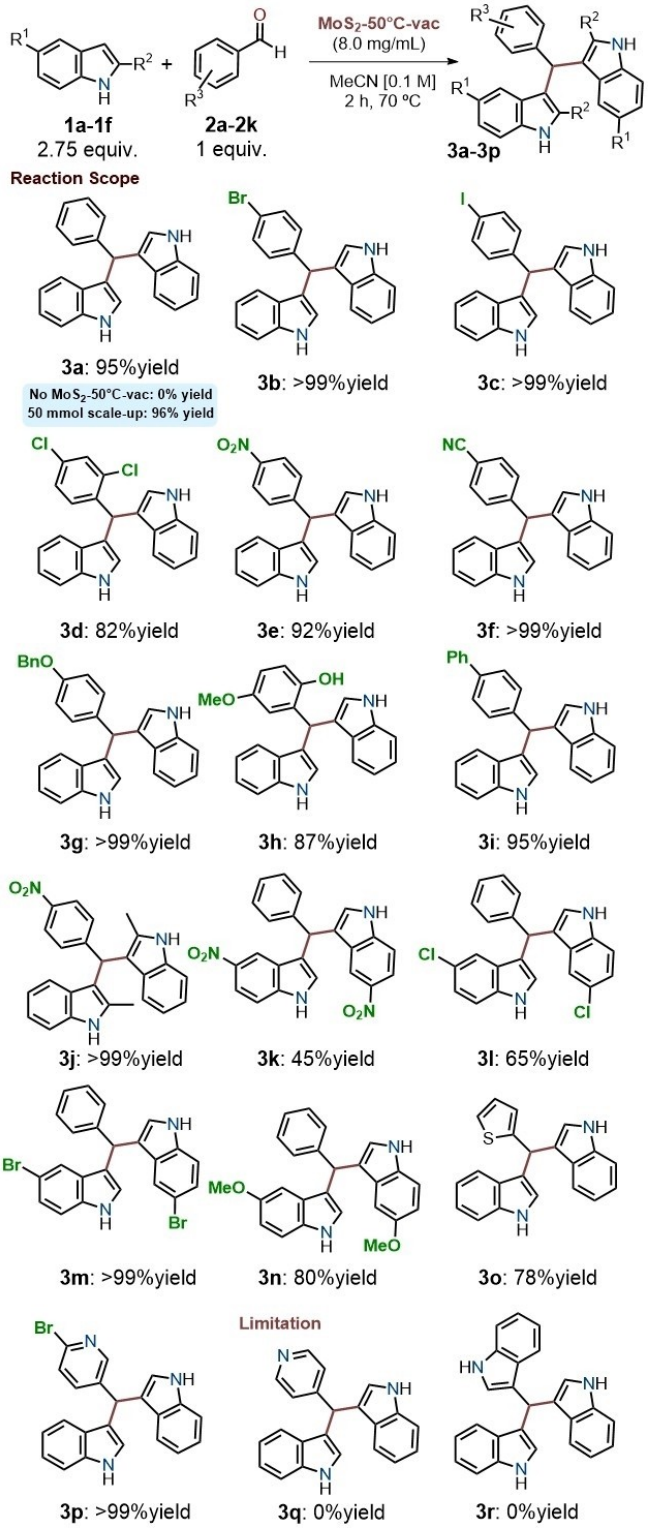

Scheme 2. Reaction scope for the MoS_2 catalysed reaction between indole **1a** and benzaldehydes **2a–k**. The reaction was performed on a 0.1 mmol scale. Yields were determined by ^{1}H-NMR using trimethoxybenzene as internal standard.

presence of electron withdrawing *para*-substituents, including bromo, iodo, cyano, and nitro groups, was well tolerated, providing the corresponding BIM derivatives in good yields. Besides, benzaldehyde bearing weak (**2i**) and strong activating groups (**2g–h**) could also be included in the reaction scope resulting in the products (**3g–i**). Indoles functionalized at position 5-(nitro, chloro, bromo and methoxy) were used in the reaction scope in the entries (**3k–3n**). Moreover, 2-methylindole **1b** could be reacted with 4-nitrobenzaldehyde to afford product **3j**. Additionally, heterocyclic aldehydes were used to obtain products **3o** and **3p**. Interestingly, the heterogenous catalyst could also be recycled by centrifugation, although a loss in catalytic activity was observed throughout the experiments (see Section 3.4 of S.I). The minor activity can be attributed to both the presence of a small amount of organic molecules on the catalyst surface after its use (Figure S18) and to the loss of material during recycling operations. Specifically, these compounds might poison the catalyst, thus decreasing its catalytic activity. The structure and morphology of the recycled catalyst were comparable to those of pristine bulk 2H–MoS_2

and MoS_2-50 °C-vac (Figures S16 and S17). Finally, the reaction scale could be increased up to 50 mmol of **2a** obtaining a yield for product **3a** of 96%.

Conclusions

In conclusion, we have demonstrated the effectiveness of the DoE approach to identify the critical parameters involved in the functionalization of indole with different benzaldehydes by using commercial bulk 2H–MoS_2 as catalyst. Importantly, it was found that 2H–MoS_2 can be straightforwardly activated by a "cleaning" of its surface based on heating under vacuum. This process serves to suitably desorb the adsorbates from MoS_2 surface, enhancing the available population of the Lewis acidic catalytic sites. Under the DoE optimized reaction conditions, the MoS_2-50 °C-vac showed to have better performances when compared with other Mo-containing materials. We believe this work will serve to make the surface cleaning treatment one general method for better activate catalytic materials prior to the catalytic tests. Besides, we provide robust evidence to encourage the use of DoE as a widely applied instrument in optimization and understanding of chemical processes.

Experimental Section

All reactions were set up in glass vials unless otherwise stated. Synthesis grade solvents were used as purchased. Chromatographic purification of products (**3a**–**i**) was accomplished using flash chromatography on silica gel (35–70 mesh). For thin layer chromatography (TLC) analysis throughout this work, Merck pre-coated TLC plates (silica gel 60 GF254, 0.25 mm) were employed, using UV light as the visualizing agent (254 nm), basic aqueous potassium permanganate ($KMnO_4$) stain solution or iodine, and heat as developing agents. Organic solutions were concentrated under reduced pressure on a Büchi rotatory evaporator. The materials utilized in catalysis were prepared according to a straightforward protocol: 100 mg of the commercially available material (MoO_2, MoS_2, and $MoSe_2$) were placed in a glass vial and subjected to vacuum for 48 h at 50 °C. Once cooled down to room temperature, the heated powder was removed from vacuum and used immediately.

Acknowledgements

M.M.-G. thanks Margarita Salas grant (MS21-041) from the Universitat de València, funded by the Spanish Ministry of Science and European Union (NextGenerationEU). G.F. and M.M. kindly acknowledge FRA2022 funded by the University of Trieste and Microgrants 2021 funded by Region FVG (LR 2/2011, ART. 4). M.P. is the AXA Chair for Bionanotechnology (2016–2023). This work was supported by the University of Trieste, INSTM, and the Italian Ministry of Education MIUR (cofin Prot. 2017PBXPN4). Part of this work was performed under the Maria de Maeztu Units of Excellence Program – Grant MDM-2017-0720.

Conflict of Interests

The authors declare no conflict of interest.

Data Availability Statement

The data that support the findings of this study are available in the supplementary material of this article.

Keywords: heterogeneous catalysis · synthetic methods · C–C coupling · molybdenum disulfide · indole derivatives

[1] K. S. Novoselov, A. Mishchenko, A. Carvalho, A. H. Castro Neto, *Science* **2016**, *353*, aac9439.
[2] J. A. Wilson, A. D. Yoffe, *Adv. Phys.* **1969**, *18*, 193–335.
[3] S. Ippolito, A. Ciesielski, P. Samorì, *Chem. Commun.* **2019**, *55*, 8900–8914.
[4] Q. H. Wang, K. Kalantar-Zadeh, A. Kis, J. N. Coleman, M. S. Strano, *Nat. Nanotechnol.* **2012**, *7*, 699–712.
[5] M. Chhowalla, H. Shin, G. Eda, L. Li, *Nat. Chem.* **2013**, *5*, 263–275.
[6] W. Choi, N. Choudhary, G. H. Han, J. Park, D. Akinwande, Y. H. Lee, *Mater. Today* **2017**, *20*, 116–130.
[7] W. Chen, W. Qi, W. Lu, N. R. Chaudhury, J. Yuan, L. Qin, J. Lou, *Small* **2018**, *14*, 1702600.
[8] I. Song, C. Park, H. C. Choi, *RSC Adv.* **2015**, *5*, 7495–7514.
[9] A. Kuc, N. Zibouche, T. Heine, *Phys. Rev. B* **2011**, *83*, 245213.
[10] P. Chandra, A. Mohammad, B. Tripathi, T. Yoon, *FlatChem* **2022**, *34*, 100395.
[11] Z. R. Zhao, H. X. Xu, X. Wang, *Synlett* **2023**, *34*, 488–492.
[12] K. Jaiswal, Y. R. Girish, M. De, *Accounts Mater. Res.* **2022**, *3*, 1033–1048.
[13] K. Jaiswal, Y. R. Girish, P. Behera, M. De, *ACS Org. Inorg. Au* **2022**, *2*, 205–213.
[14] Y. M. Wang, W. J. Li, M. M. Wang, M. Zhang, Z. H. Zhang, *Catal. Sci. Technol.* **2023**, *13*, 665–674.
[15] M. Breysse, G. Berhault, S. Kasztelan, M. Lacroix, F. Maugé, G. Perot, *Catal. Today* **2001**, *66*, 15–22.
[16] S. Rangarajan, M. Mavrikakis, *ACS Catal.* **2017**, *7*, 501–509.
[17] X. Sun, X. Zhang, Y. Xie, *Matter* **2020**, *2*, 842–861.
[18] A. Wang, J. Li, T. Zhang, *Nat. Chem. Rev.* **2018**, *2*, 65–81.
[19] C. Vogt, B. M. Weckhuysen, *Nat. Chem. Rev.* **2022**, *6*, 89–111.
[20] A. Bahuguna, S. Kumar, V. Sharma, K. L. Reddy, K. Bhattacharyya, P. C. Ravikumar, V. Krishnan, *ACS Sustainable Chem. Eng.* **2017**, *5*, 8551–8567.
[21] M. Shiri, M. A. Zolfigol, H. G. Kruger, Z. Tanbakouchian, *Chem. Rev.* **2010**, *110*, 2250–2293.
[22] R. M. N. Kalla, S. C. Hong, I. Kim, *ACS Omega* **2018**, *3*, 2242–2253.
[23] H. Ramshini, B. Mannini, K. Khodayari, A. Ebrahim-Habibi, A. S. Moghaddasi, R. Tayebee, F. Chiti, *Eur. J. Med. Chem.* **2016**, *124*, 361–371.
[24] E. Reyes-Mercado, J. A. Rivas-Loaiza, J. P. García-Merinos, Y. López, J. B. González-Campos, *Chem. Eng. Process. Process Intensif.* **2021**, *159*, 108201.
[25] C. Ramesh, J. Banerjee, R. Pal, B. Das, *Adv. Synth. Catal.* **2003**, *345*, 557–559.
[26] M. Chakrabarty, N. Ghosh, R. Basak, Y. Harigaya, *Tetrahedron Lett.* **2002**, *43*, 4075–4078.
[27] M. Karthik, A. K. Tripathi, N. M. Gupta, M. Palanichamy, V. Murugesan, *Catal. Commun.* **2004**, *5*, 371–375.
[28] V. Nori, A. Sinibaldi, G. Giorgianni, F. Pesciaioli, F. Di Donato, E. Cocco, A. Biancolillo, A. Landa, A. Carlone, *Chem. A Eur. J.* **2022**, *28*, e202104524.
[29] B. MacQueen, R. Jayarathna, J. Lauterbach, *Curr. Opin. Chem. Eng.* **2022**, *36*, 100781.
[30] R. Leardi, *Anal. Chim. Acta* **2009**, *652*, 161–172.
[31] V. Czitrom, *Am. Stat.* **1999**, *53*, 126–131.
[32] B. Dejaegher, Y. Vander Heyden, *J. Pharm. Biomed. Anal.* **2011**, *56*, 141–158.
[33] D. W. Lendrem, B. C. Lendrem, D. Woods, R. Rowland-Jones, M. Burke, M. Chatfield, J. D. Isaacs, M. R. Owen, *Drug Discovery Today* **2015**, *20*, 1365–1371.
[34] S. N. Politis, P. Colombo, G. Colombo, D. M. Rekkas, *Drug Dev. Ind. Pharm.* **2017**, *43*, 889–901.

[35] T. S. Singh, T. N. Verma, *Energy Convers. Manage.* **2019**, *182*, 383–397.
[36] B. Macqueen, E. Barrow, G. Rivera Castro, Y. Pagan-Torres, A. Heyden, J. Lauterbach, *Ind. Eng. Chem. Res.* **2019**, *58*, 8681–8689.
[37] G. D. Bowden, B. J. Pichler, A. Maurer, *Sci. Rep.* **2019**, *9*, 11370.
[38] P. M. Murray, F. Bellany, L. Benhamou, D. K. Bučar, A. B. Tabor, T. D. Sheppard, *Org. Biomol. Chem.* **2016**, *14*, 2373–2384.
[39] Q. Yue, Z. Shao, S. Chang, J. Li, *Nanoscale Res. Lett.* **2013**, *8*, 425.
[40] S. Zhao, J. Xue, W. Kang, *Chem. Phys. Lett.* **2014**, *595*, 35–42.
[41] E. Mitterreiter, B. Schuler, A. Micevic, D. Hernangómez-Pérez, K. Barthelmi, K. A. Cochrane, J. Kiemle, F. Sigger, J. Klein, E. Wong, E. S. Barnard, K. Watanabe, T. Taniguchi, M. Lorke, F. Jahnke, J. J. Finley, A. M. Schwartzberg, D. Y. Qiu, S. Refaely-Abramson, A. W. Holleitner, A. Weber-Bargioni, C. Kastl, *Nat. Commun.* **2021**, *12*, 3822.
[42] Y. Beckmann, A. Grundmann, L. Daniel, M. Abdelbaky, C. McAleese, X. Wang, B. Conran, S. Pasko, S. Krotkus, M. Heuken, H. Kalisch, A. Vescan, W. Mertin, T. Kümmell, G. Bacher, *ACS Appl. Mater. Interfaces* **2022**, *14*, 35184–35193.
[43] N. J. Mayhall, E. L. Becher, III, A. Chowdhury, K. Raghavachari, *J. Phys. Chem. A* **2011**, *115*, 2291–2296.
[44] P. K. Samantaray, S. Indrakumar, K. Chatterjee, V. Agarwal, S. Bose, *Nanoscale Adv.* **2020**, *2*, 2824–2834.
[45] C. Lee, H. Yan, L. E. Brus, T. F. Heinz, J. Hone, S. Ryu, *ACS Nano* **2010**, *4*, 2695–2700.
[46] E. Er, H.-L. Hou, A. Criado, J. Langer, M. Möller, N. Erk, L. M. Liz-Marzán, M. Prato, *Chem. Mater.* **2019**, *31*, 5725–5734.

Manuscript received: June 10, 2023
Revised manuscript received: July 24, 2023
Accepted manuscript online: July 24, 2023
Version of record online: August 21, 2023